An Integrated Technique for Fault Location and Section Identification in Distribution Systems

D.S. Gazzana, G.D. Ferreira, A.S. Bretas, A.L. Bettiol, A. Carniato, L.F.N. Passos, A.H. Ferreira, J.E.M. Silva

Abstract-- **The paper proposes an integrated impedance and transient-based fault location formulation taking into account unbalanced operation, presence of intermediate loads, laterals, and time-varying load profile. Considering the fault distance obtained from the proposed extended impedance method, the transient analysis of the faulted signal is evaluated. Based on high frequency analysis, the location of the faulty section can be identified by eliminating the multiple estimative of the fault location obtained from the impedance-based method. Aiming to verify the application of the proposed methodology, simulations were carried out in the ATP Software considering a simple configuration and a real electric power distribution system (above 200 buses).**

Keywords: **Apparent impedance, distribution network, fault location, transient analysis.**

I. INTRODUCTION

Several techniques have been proposed in the literature in order to identify the fault location in distribution systems. Some established methods, such as those based on apparent impedance, are able to identify with acceptable accuracy the fault distance in relation to the local terminal [1]-[2]. However, as the distribution systems have multiple branches and the voltage and current measurements are usually available only at the substation, the location of the faulty section is a problem not solved yet. Currently, this is a great challenge related to the fault location study.

Impedance-based fault location techniques for distribution systems are especially attractive because of their low implementation cost, particularly one-terminal-based ones [3]-[11]. However, most of these methods do not consider the characteristics of distribution systems (unbalanced operation, presence of intermediate loads, laterals, and time-varying load profile), which significantly affect their performance. This intrinsic characteristic of electric power distribution systems

has a detrimental effect on the accuracy of the fault locators, since the load data during the fault period is a required input for any impedance-based method. Distribution systems lines are typically overhead and of relatively short length. For these reasons, very few impedance-based fault location techniques have considered the shunt capacitance of distribution lines in conjunction with its inherent unbalance [12]. However, in the cases of long, lightly loaded overhead lines as well as underground feeders, the shunt admittance should be included [13].

The techniques based on the transient signals, with focus on high frequency analysis can be considered the state-of-the-art to solve the problem of multiple estimates of fault location. A fault occurring in a distribution feeder generates a traveling wave which propagates through the system. It is reflected several times in the fault point and in the other terminals. This transient of high frequency has characteristic spectral components according to the fault location, which can be identified using mathematical procedures for time-frequency analysis [14]-[16]. These analyses can contribute to identify the faulty section of the feeder, eliminating the multiple estimates of the fault location.

In this context, the focus of this paper is to establish a hybrid methodology based on the apparent impedance and transient analysis in order to estimate the fault distance and the fault location in distribution systems.

II. FAULT LOCATION BASED ON APPARENT IMPEDANCE ANALYSIS

The proposed method for fault distance estimation is based on the analysis of apparent impedance (AI) seen from local terminal during the pre-fault and fault periods. The method uses pre-fault values in order to both compensate load uncertainty and compute equivalent systems for each possible path from local terminal to the fault point. Fault-period signals are analyzed in order to estimate the fault distance for each equivalent system. The methodology is illustrated in Fig. 1.

In describing the techniques represented in Fig. 1 the following notations are adopted in this paper:
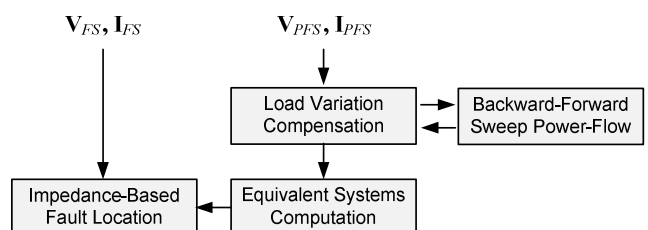
D. S. Gazzana, G. D. Ferreira, A. S. Bretas are with Department of Electrical Engineering, UFRGS University, Porto Alegre (RS), Brazil (e-mail: dgazzana@ece.ufrgs.br, gustavoferreira@ece.ufrgs.br, abretas@ece.ufrgs.br).

A. L. Bettiol, A. Carniato, L. F. N. Passos are with A Vero Domino Consulting and Research, Florianópolis (SC), Brazil (e-mail: arlan@averodomino.com.br, carniato@averodomino.com.br, luis@averodomino.com.br).

A. H. Ferreira is with CETRIL, Ibiúna (SP), Brazil (e-mail: alberto@cetril.com.br).

J. E. M. Silva is with EFLJC, Siderópolis (SC), Brazil (e-mail: joseemerson@joaocesa.com.br).

Fig. 1. Flowchart of the proposed AI method.

$\mathbf{V}_{PFS} = [V_{PFSa} \ V_{PFSb} \ V_{PFSc}]^T$ pre-fault voltage at the source node (V);

$\mathbf{I}_{PFS} = [I_{PFSa} \ I_{PFSb} \ I_{PFSc}]^T$ pre-fault current at the source node (A);

$\mathbf{V}_{FS} = [V_{FSa} \ V_{FSb} \ V_{FSc}]^T$ fault voltage at the source node (V);

$\mathbf{I}_{FS} = [I_{FSa} \ I_{FSb} \ I_{FSc}]^T$ fault current at the source node (A);

$\mathbf{V}_F = [V_{Fa} \ V_{Fb} \ V_{Fc}]^T$ voltage at the fault point (V);

$\mathbf{I}_F = [I_{Fa} \ I_{Fb} \ I_{Fc}]^T$ fault current at the fault point (A);

R_{Fk} fault resistance of phase k (Ω);

$\mathbf{Z}$ third-order line series impedance matrix (Ω /m);

$\mathbf{Y}$ third-order line shunt admittance matrix (S/m);

$\mathbf{I}_x = [I_{xa} \ I_{xb} \ I_{xc}]^T$ current at the lumped line impedance upstream from the fault point (A);

$\mathbf{I}_D = [I_{Da} \ I_{Db} \ I_{Dc}]^T$ current downstream from the fault point (A);

$\mathbf{Z}_{eqn}$ equivalent node impedance matrix (Ω);

$\mathbf{Z}^L_{eqn}$ equivalent node load impedance matrix (Ω);

ℓ line length (m);

x fault distance (m).

A. Load Variation Compensation

Although the system load impedances are assumed to be available for the fault location they can hardly represent exact values, since there is a degree of uncertainty in the loading estimation. Thus, the first step is to compensate the load uncertainties in order to reduce the error in the fault distance estimation. By knowing the pre-fault voltages and currents, the apparent impedance seen from the local terminal can be computed as

$$Z_{PFSk} = V_{PFSk}/I_{PFSk}, \tag{1}$$

for $k = a, b, c$.

By using the back-forward sweep power-flow described in [13], the estimated current at the local node (I'_{PFSk}) is determined. Thus, the estimated pre-fault impedance (Z'_{PFk}) is computed, as

$$Z'_{PFSk} = V_{PFSk}/I'_{PFSk}. \tag{2}$$

The load variation factors associated to the active (ΔR_k) and reactive (ΔX_k) components of load impedances are given by:

$$\Delta R_k = \left(\Re\{Z_{PFk}\} - \Re\{Z'_{PFk}\}\right)/\Re\{Z'_{PFk}\} \tag{3}$$

$$\Delta X_k = \left(\Im\{Z_{PFk}\} - \Im\{Z'_{PFk}\}\right)/\Im\{Z'_{PFk}\}, \tag{4}$$

where $\Re\{\cdot\}$ and $\Im\{\cdot\}$ denote the real and imaginary parts of a complex number, respectively. Compensation of load variations is performed by multiplying the real and imaginary
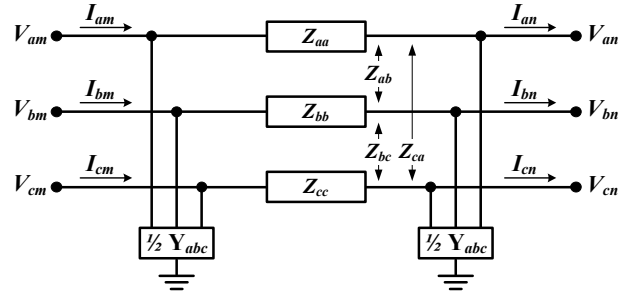

Fig. 2. Exact line segment model.

parts of load matrices by $(1+\Delta R_k)$ and $(1+\Delta X_k)$, respectively.

The described procedure is repeated, by running the power-flow and applying (2)-(4) until the impedances given by (1) and (2) match. Convergence can be verified if

$$\max_k \left(|\Delta R_k|\right) \le \varepsilon \quad \text{and} \quad \max_k \left(|\Delta X_k|\right) \le \varepsilon, \tag{5}$$

where ε is a predefined tolerance.

B. Equivalent Systems Computation

The computation of equivalent systems is performed in order to make the AI method suitable for application in distribution feeders with arbitrary number of lateral branches and loads. The technique consists in for each possible path from the local node to a fault point, to obtain equivalent impedances for lines and loads outside the analyzed path. By considering the system pre-fault conditions, the equivalent impedance of phase k is calculated for each feeder node n, according to:

$$Z_{eq\,nk} = V_{nk}/I_{(m-n)k}, \tag{6}$$

where V_{nk} is the pre-fault node voltage and $I_{(m-n)k}$ is the current flowing from the upstream node m to node n. If node n is a connection point for a lateral or load then the equivalent *load* impedance for each phase k ($Z^L_{eq\,nk}$) is also calculated:

$$Z^L_{eq\,nk} = V_{nk}/\left(I_{(m-n)k} - I_{(n-p)k}\right), \tag{7}$$

where $I_{(n-p)k}$ is the current flowing from the node n to the downstream node p.

C. Equations for Fault Distance Estimation

The mathematical formulation of the proposed AI method is derived from the exact line segment model [13], shown in Fig. 2. This model was chosen because it is suitable for representing untransposed overhead and underground (highly capacitive) distribution lines. It is also more accurate in case of long, lightly loaded (rural) distribution systems, where capacitive currents are of considerable magnitude [2].

Consider a fault occurring in a distribution line of length ℓ, represented by the model of Fig. 2. If the fault occurs at a distance x from the source terminal, the resulting voltage at the fault point ($\mathbf{V}_F$) can be expressed as (8):

$$\mathbf{V}_F = \mathbf{V}_{FS} - x \cdot \mathbf{Z} \cdot \mathbf{I}_x. \tag{8}$$

For a three-phase to ground fault, the voltage at the fault

point for each phase k can be expressed as

$$V_{Fk} = R_{Fk} \cdot I_{Fk} + R_{Fg} \cdot I_{Fg}, \tag{9}$$

where $I_{Fg} = I_{Fa} + I_{Fb} + I_{Fc}$. Equation (9) can be generalized for any type of fault involving one or more phases and ground, by making the currents on the healthy phases equal to zero. Replacing (8) in (9), it is possible to write (10) for each faulted phase k:

$$R_{Fk} \cdot I_{Fk} + R_{Fg} \cdot I_{Fg} = V_{FSk} - x \cdot M_k, \tag{10}$$

where M_k is the k-th row of the matrix $\mathbf{M} = \mathbf{Z} \cdot \mathbf{I}_x$.

By separating (10) into its real and imaginary parts, it can be found that

$$R_{Fk} \cdot I_{Fk}^r + R_{Fg} \cdot I_{Fg}^r = V_{FSk}^r - x \cdot M_k^r \tag{11}$$

$$R_{Fk} \cdot I_{Fk}^i + R_{Fg} \cdot I_{Fg}^i = V_{FSk}^i - x \cdot M_k^i \tag{12}$$

where the superscripts r and i denote the real and imaginary parts of the variables, respectively. By isolating R_{Fk} in (11), replacing in (12) and rearranging its terms it is possible to obtain (13):

$$x \cdot \left(M_k^r \cdot I_{Fk}^i - M_k^i \cdot I_{Fk}^r \right) + V_{FSk}^i \cdot I_{Fk}^r - V_{FSk}^r \cdot I_{Fk}^i \\ - R_{Fg} \cdot \Im \left\{ I_{Fg} \cdot I_{Fk}^* \right\} = 0 \tag{13}$$

Equation (13) can be written for each faulted phase k. The sum of the resulting equations is a single generalized equation, which can be used to estimate the fault distance x for all types of ground faults. Considering that $\Im \left\{ I_{Fg} \cdot I_{Fg}^* \right\} = 0,$ the final form of (13) is given by (14):

$$x = \sum_{k \in \Theta} \Im \left\{ V_{FSk} \cdot I_{Fk}^* \right\} \Big/ \sum_{k \in \Theta} \Im \left\{ M_k \cdot I_{Fk}^* \right\} \tag{14}$$

where Θ is the set of faulted phases, given by any combination of phases a, b and c.

For phase-to-phase faults, similar steps to those used to obtain (15) are followed. However, $I_{Fg} = 0$ in (9), and (10) is a single equation given by:

$$V_{FSj} - x \cdot M_j = V_{FSk} - x \cdot M_k + R_F \cdot I_{Fk}, \tag{15}$$

where j and k are the faulted phases. The resulting generalized fault distance equation for phase faults is expressed by (16):

$$x = \Im \left\{ \left(V_{FSk} - V_{FSj} \right) \cdot I_{Fk}^* \right\} \Big/ \Im \left\{ \left(M_k - M_j \right) \cdot I_{Fk}^* \right\}. \tag{16}$$

Equations (14) and (16) give the fault distance x as a function of both the fault current (I_{Fk}) and the current flowing through the line impedance upstream from the fault (I_{xk}). Since these variables are unknown from the local terminal measurements, they are estimated by an iterative procedure.

By starting with $x = \ell/2$ as a first estimation of the fault distance, the unknown variable $\mathbf{I}_x$ can be estimated considering compensation of the capacitive current flowing through the line shunt admittance, according to:

$$\mathbf{I}_x = \mathbf{I}_{FS} - 0.5 \cdot x \cdot \mathbf{Y} \cdot \mathbf{V}_{FS}. \tag{17}$$

The current $\mathbf{I}_F$ is the difference between the current $\mathbf{I}_x$ (upstream from the fault point) and the sum of the load current ($\mathbf{I}_D$) and the capacitive current flowing through the shunt admittance lumped at the fault point. It is expressed as

$$\mathbf{I}_F = \mathbf{I}_x - \left(0.5 \cdot x \cdot \mathbf{Y} \cdot \mathbf{V}_F + \mathbf{I}_D \right) \tag{18}$$

where

$$\mathbf{I}_D = \mathbf{Y}_D \cdot \mathbf{V}_F, \tag{19}$$

and $\mathbf{Y}_D$ is the equivalent admittance downstream from the fault point, given by

$$\mathbf{Y}_D = \left\{ (\ell - x) \cdot \mathbf{Z} + \left[0.5 \cdot (\ell - x) \cdot \mathbf{Y} + \mathbf{Z}_{eq}^{-1} \right]^{-1} \right\}^{-1} \\ + 0.5 \cdot (\ell - x) \cdot \mathbf{Y}. \tag{20}$$

Once current $\mathbf{I}_F$ is obtained, the fault distance can be estimated using (14) for a ground fault or (16) for phase-to-phase fault. From the new estimate of x, a new current $\mathbf{I}_x$ is obtained and the procedure repeated by applying (18)-(20) until convergence is attained. In this paper convergence is considered by testing the following condition:

$$\left| x^{iter-1} - x^{iter} \right| \le \delta, \tag{21}$$

where $iter$ is an iteration counter, and δ is a predefined tolerance. The procedure outlined above are applied to each equivalent system computed as explained in Section II-B.

III. Fault Location Based on Transient Analysis

A fault occurring in a distribution feeder generates a traveling wave which propagates through the system. It is reflected several times in the fault point and in the other terminals. This transient of high frequency has characteristic spectral components according to the fault location. The essential idea of this approach is to establish a correlation between characteristic frequencies associated with a specific path where the traveling wave propagates in the occurrence of a fault [14]. These spectral components are correlated with theoretical frequencies, calculated for each possible path of the wave propagation. The transient analyses can contribute to identify the faulty section of the feeder, eliminating the multiple estimates of the fault location. To understand the problem it is considered the system presented in the Fig.3.

Based on the apparent impedance methodology presented previously, which is able to establish the fault distance with measurement in one terminal, several distances estimations are determined. For instance, in the system shown in Fig. 3, if the distance was estimated around 2.3 km the fault could have occur in the point P1 or P2.

It is known that electromagnetic phenomena present in a line propagate as a traveling wave. Any temporal variation in the operation parameters of the line will be propagated as a wave. A fault results mainly in a suddenly change in the voltages and currents in a point of the line [17]. Consequently,
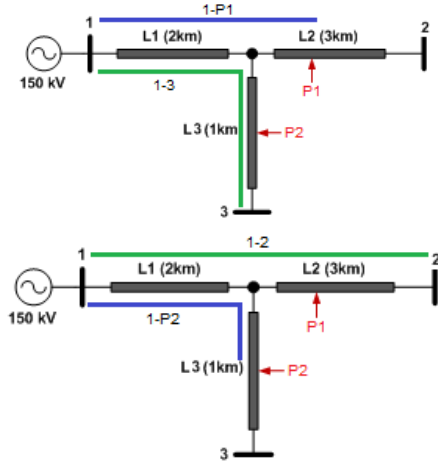
Fig. 3. Paths of the traveling wave associated to a fault. Top: fault in P1, Bottom: fault in P2.

TABLE I
CHARACTERISTIC FREQUENCIES FOR FAULT OCCURRED IN P1.

Path	x (km)	n_p	f_c (kHz)
1-P1	2.3	4	32.6
1-3	3	2	50

TABLE II
CHARACTERISTIC FREQUENCIES FOR FAULT OCCURRED IN P2.

Path	x (km)	n_p	f_c (kHz)
1-P2	2.3	4	32.6
1-3	5	2	30

a traveling wave will be propagated until find a discontinuity in the medium. Part of this will be reflected several times in the fault point and in the other terminals (discontinuities) until the steady state. This transient of high frequency has spectral characteristics according to the fault location, which can be identified using a time-frequency transformation.

With this concept, if the fault occurs in the point P1 two possible paths for the traveling wave are possible: path 1-P1 and path 1-3 as can be seen in Fig. 3 (top). If the fault occurs in P2 the paths 1-P2 and 1-2 are verified.

According to [14], the characteristic frequency f_c associated with each path p can be determined by (22)

$$f_{ct} = \frac{v}{n_p \cdot x} \tag{22}$$

where: v is the wave propagation velocity (km/s); x is the fault distance (km) and n_p is the reflection coefficient of the path p.

In (22) n_p can be equal to 2 or 4 depending of the polarity of the reflection coefficient in the extremities of the analyzed lateral. In accordance with this definition, the coefficient in the fault point can be considered close to -1 because the fault resistance has low values in comparison with the line impedance. In the measurement point, the coefficient assumes value equal to +1 because the short-circuit impedance of the system is higher than the network impedance. Based on these definitions, n_p will be equal to 2 for the paths 1-2 and 1-3. For the paths 1-P1 and 1-P2 n_p assumes 4.

Using (22) and considering v as the light speed, it can be determined the characteristics frequencies for each path presented in Fig. 3. Tables I and II presents these frequencies for a fault occurred in the points P1 and P2 respectively.

Analyzing the results presented in Tables I and II, in a case that the fault distance of more than two possible paths are the same, it is verified that the component associated to the line length is the frequency responsible for the identification of the faulted section. It can be stated that, depending of the fault resistance, the characteristic frequency associated with the length of the branch in fault do not appear in the frequency spectrum or its magnitude should have low energy.

To summarize, in the proposed example for a fault occurred in P1 a frequency component associated to the path 1-2 (30 kHz) should have magnitude close to zero or smaller than the magnitude of the path 1-3 (50 kHz). Otherwise, if the fault occurs in P2, the magnitude of the frequency related to the path 1-3 (50 kHz) should be inexpressive or smaller than the spectral energy of the 30 kHz component associated to the path 1-2. In accordance with this concept, the fault section can be better identified taking into account multiple estimates of the fault location originated from the impedance apparent algorithm.

A. Numerical Implementation

The proposed methodology to identify the faulty section is based on six steps: fault detection; modal transformation; signal filtering; characteristic frequency identification; transient analysis and faulty section identification.

The first step in order to identify the faulty section corresponds to a correct identification of the disturbance onset recorded by the digital oscillograph. A disturbance is characterized by distortions in the waveform of the voltage and current in relation to the pre-fault condition as a change in angle and magnitude. Thus, the determination of the initial instant of the transient can be performed by comparison between actual and past samples. To this purpose, the Park's transformation can be used [18].

The modal decomposition of the phase voltage signals is accomplished by the use of Clarke's matrix. It is noteworthy that this matrix is ideally used for symmetrical lines or fully transposed systems. Based on several simulations for different types of fault (phase-ground, phase-phase, 2 phase-ground and 3 phase- ground) and different values of fault resistance, it was found that the propagation modes 0, 1 and 2 have better applicability depending on the type of fault. Thus, it was found that: propagation mode 0 has better applicability for phase-ground and 2 phase-ground faults; propagation mode 1 has better applicability for phase-phase faults; propagation mode 2 has better applicability for 3 phase-ground and phase-phase faults.

Assuming that in the transient signal the spectral component with greatest magnitude is the fundamental frequency (60 Hz), it is necessary to remove this component due to its high energy compared to other frequency present in the signal related to the possible paths of the traveling wave generated by the fault. Thus, the use of a high-pass filter has a

substantial importance to ensure that the several components associated with the fault can be evaluated in an acceptable energy scale, improving the performance in the signal processing task. In the proposed method, it was adopted a high-pass filter type Butterworth, order 10 with cutoff frequency of 300 Hz.

By knowing the fault distance obtained by the apparent impedance method presented previously, it can be determined the n sections in the distribution system, which can be associated with the fault. For each section, the total length of the line segment should be identified, which is characterized by the first discontinuity (change of cable, load, transformer). This length is defined as the length of the section. Thus, using (22), n frequencies will be evaluated associated with the length of the p paths.

In the proposed method, the analysis of the transient fault signal is performed in the frequency domain (FD). In this context, the Fourier Transforms, Wavelet, Gabor can be used. The essential idea is to find the components associated with each section and evaluate such magnitudes. Based on several simulations it was found that all mentioned methods identify the same frequency components associated with the paths of the traveling wave. Thus, the different time-frequency methodologies presented similar performance to the identification of the faulty section.

Finally, the faulty section is identified based on comparison of the magnitudes of frequency components associated with each path p for the approach FD. The frequency component associated with the path that presents the high magnitude of the fault distance and the less magnitude of the section length will indicate the occurrence of the section in fault. Based on these magnitudes, a probabilistic estimation is inferred for all possible sections in fault.

IV. SIMULATION RESULTS

In order to check the robustness of the proposed methodology, simulations in ATP software were carried out with base on a simple system and a real distribution network.

A. Simple Configuration

In this study, two possible faulty sections were considered, as can be seen in Fig. 4. The possible points for the fault (FL1 and FL2) have the same distance in relation to the measurement terminal (400m).

Different types of faults (Ag, Bg, Cg, ABg, BCg, ACg, AB, BC, CA, ABCg) with resistance equal to 0 Ω, 10 Ω, 50 Ω and 100 Ω in the points FL1 and FL2 were evaluated resulting in 80 scenarios. Table III summarizes the performance of the method.
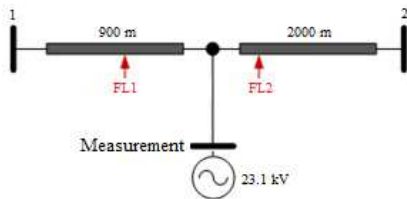

Fig. 4. System configuration used in the tests.

TABLE III
PERFORMANCE OF THE TRANSIENT ANALYSIS METHOD

3 Phase-ground (8 cases)	Phase-ground and 2 Phase-ground (48 cases)	Phase-phase (24 cases)
Agreement (%)		
100	100	100

Based on the results it can be stated that the proposed methodology can identify the faulty section without errors. However, the following observation must be done:
- the accuracy of the algorithm is related to the number of section that could be in fault. With the increase in the number of paths of the traveling wave, the number of the reflections increases too causing the appearance of several components in the spectrum that can overlap the interest frequencies;
- the system load can affect the performance of the algorithm because the load is a discontinuity. Depending of its characteristics, the reflected waves can be attenuated reducing the accuracy of the method;
- with the increase of the paths associated to the traveling wave, the fault resistance can affect the location of the faulty section.

B. Real Distribution Network

A second group of simulations was performed considering a real distribution feeder located in southern Brazil (Siderópolis - SC). The feeder has an equivalent circuit of 241 buses, total line length of 19.4 km and average load demand of 3.15 MVA. The result of the transient analysis is presented as a probability for each estimated location performed by the apparent impedance method. The Google Earth view of the real feeder can be seen in Fig. 5.
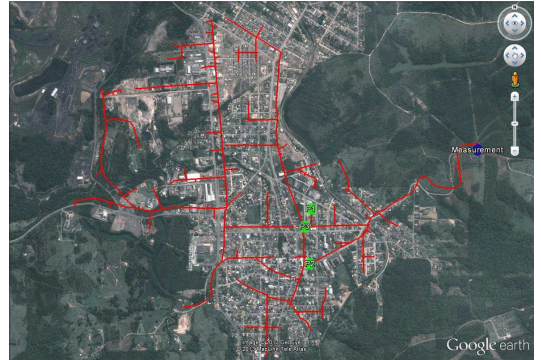

Fig. 5. Google Earth view of the real distribution feeder.

Four fault scenarios were selected to illustrate the application of the proposed hybrid technique for fault distance and faulted section identification. Table IV summarizes the fault distances estimated by the impedance-based algorithm and the respective probabilities given by the transient analysis. The fault distances for each location are in relation to the local terminal ("measurement" point in Fig. 5).

In the results presented in the Table IV the bold lines corresponds to the point where the fault occurs. It can be noted that the apparent impedance algorithm estimates different possible fault locations ranging from three to nine and the transient analysis inferred a probability for each location.

If the number of possible locations increases it becomes more difficult to establish a reliable probability for the correct one. For instance, in the case 1 only three possibilities of the fault location was estimated and the highest probability (42.4%) to the point P3 corresponds to the fault location.

Otherwise, in the case 3 the transient analysis determinates the highest probability (12.2%) for points P4 and P7. However, the fault occurred in the point P9, to which the assigned probability was 12.1%.

The AI method proved effective in estimating the fault distances in the simulated fault scenarios. For the four cases shown in Table IV the correct distances are 1730.4, 3047.7, 2555.5 and 3284.5 m from the local terminal, respectively. The resulting percent error for each case are 0.32 %, 0.71 %, $2.06 \ 10^{-3}$ % and $5.14 \ 10^{-4}$ %, respectively. Table V summarizes the results obtained from the 80 simulated fault scenarios. Results are presented in terms of the average, maximum, minimum and standard deviation values of percent errors in the fault distance estimate.

V. CONCLUSIONS

In this work was presented aspects regarding the developed methodology for identifying the faulty section in distribution systems. With the knowledge of the type and the fault distance, determined by the apparent impedance method, a technique based on traveling waves and transient analysis can estimate, in a probability way, the section of the feeder in fault.

The paper proposed a hybrid impedance and transient-based fault location formulation taking into account unbalanced operation, presence of intermediate loads, laterals, and time-varying load profile. Different of some methods which use association of series and parallel impedances, the proposed apparent impedance technique relies on a power flow in order to determine such equivalent systems. The advantage of this approach is that it considers the asymmetrical line coupling and is more efficient for application in large distribution networks.

Based on high frequency analysis, the location of the faulty section can be better identified by eliminating the multiple estimative of the fault location obtained from the impedance-based method. However, its performance is dependent of the number of sections, fault resistance and the loads present in the system. It was verified that the characteristic frequencies determined by (22) sometimes needs a correction in order to improve the fault location. Additionally, high impedance faults shown to be more difficult to detect. It is worth to mention that all the developed techniques use only one-terminal measurements.

VI. ACKNOWLEDGMENT

TABLE IV
RESULTS CONSIDERING A REAL DISTRIBUTION FEEDER

Case 1: Fault type Ag with resistance of 10 Ω		
Location	Fault distance (m)	Probability (%)
P1	1667.5	28.8
P2	1730.3	28.8
P3	**1667.1**	**42.4**
Case 2: Fault type AB with resistance of 10 Ω		
Location	Fault distance (m)	Probability (%)
P1	2897.1	10.2
P2	2755.1	10.6
P3	**2909.4**	**16.1**
P4	2889.5	15.8
P5	2784.8	15.7
P6	2875.4	15.8
P7	2875.7	15.8
Case 3: Fault type BCg with resistance of 0 Ω		
Location	Fault distance (m)	Probability (%)
P1	2647.9	8.0
P2	2555.9	8.0
P3	2621.3	12.0
P4	2712.2	12.2
P5	2693.5	11.9
P6	2556.4	11.7
P7	2694.9	12.2
P8	2701.5	11.9
P9	**2555.9**	**12.1**
Case 4: Fault type ABCg with resistance of 0 Ω		
Location	Fault distance (m)	Probability (%)
P1	2453.3	9.7
P2	2621.3	9.7
P3	3129.4	15.6
P4	3270.3	16.1
P5	3319.9	16.1
P6	3281.1	16.1
P7	**3284.6**	**16.7**

TABLE V
ERROR STATISTICS FOR THE FAULT DISTANCE ESTIMATES.

Fault Distance Estimation Error (%)			
Average	Maximum	Minimum	Std. Deviation
0.022	0.089	0.000	0.025

VII. REFERENCES

[1] A. D. Filomena, M. Resener, R. H. Salim, and A. S. Bretas, "Fault location for underground distribution feeders: An extended impedance-based formulation with capacitive current compensation," *International Journal of Electrical Power & Energy Systems*, vol. 31, pp. 489-496, Oct 2009.

[2] R. H. Salim, K. C. O. Salim, and A. S. Bretas, "Further improvements on impedance-based fault location for power distribution systems," *IET Generation Transmission & Distribution*, vol. 5, pp. 467-478, Apr 2011.

[3] M.-S. Choi, S.-J. Lee, S.-I. Lim, D.-S. Lee, and X. Yang, "A direct three-phase circuit analysis-based fault location for line-to-line fault," *IEEE Transactions on Power Delivery*, vol. 22, pp. 2541-2547, Oct 2007.

[4] R. H. Salim, M. Resener, A. D. Filomena, K. R. Caino de Oliveira, and A. S. Bretas, "Extended Fault-Location Formulation for Power Distribution Systems," *IEEE Transactions on Power Delivery*, vol. 24, pp. 508-516, Apr 2009.

[5]   Zhu, D. L. Lubkeman, and A. A. Girgis, "Automated fault location and diagnosis on electric power distribution feeders," *IEEE Transactions on Power Delivery*, vol. 12, pp. 801-809, Apr 1997.

[6]   S. J. Lee, M. S. Choi, S. H. Kang, B. G. Jin, D. S. Lee, B. S. Ahn, N. S. Yoon, H. Y. Kim, and S. B. Wee, "An intelligent and efficient fault location and diagnosis scheme for radial distribution systems," *IEEE Transactions on Power Delivery*, vol. 19, pp. 524-532, Apr 2004.

[7]   R. Das, M. S. Sachdev, and T. S. Sidhu, A technique for estimating locations of shunt faults on distribution lines, 1995.

[8]   R. Das, M. S. Sachdev, and T. S. Sidhu, A fault locator for radial subtransmission and distribution lines, 2000.

[9]   D. Novosel, D. Hart, Y. Hu, and J. Myllymaki, "System for locating faults and estimating fault resistance in distribution networks with tapped loads," 1998.

[10]   M. S. Choi, S. J. Lee, D. S. Lee, and B. G. Jin, "A new fault location algorithm using direct circuit analysis for distribution systems," *IEEE Transactions on Power Delivery*, vol. 19, pp. 35-41, Jan 2004.

[11]   Y. Liao, "Generalized Fault-Location Methods for Overhead Electric Distribution Systems*," IEEE Transactions on Power Delivery*, vol. 26, pp. 53-64, Jan 2011.

[12]   M. M. Saha, J. Izykowski, and E. Rosolowski, *Fault location on power networks*. London: Springer-Verlag, 2010.

[13]   W. H. Kersting, *Distribution System Modeling and Analysis*. Boca Ratón, FL: CRC Press, 2002.

[14]   A. Borghetti, S. Corsi, C.A. Nucci, M. Paolone, L. Peretto, and R. Tinarelli, "On the use of continuous-wavelet transform for fault location in distribution power systems," *International Journal of Electrical Power and Energy Systems*, vol. 28, pp. 608-617, Mar 2006.

[15]   A. Borghetti, M. Bosetti, M. Di Silvestro, C.A. Nucci and M. Paolone, "Continuous-wavelet transform for fault location in distribution power networks: definition of mother wavelets inferred from fault originated transients," *IEEE Transactions on Power System*, vol. 23, n. 2, pp. 380-388, May 2008.

[16]   A. Borghetti, M. Bosetti, C.A. Nucci, M. Paolone and A. Abur, "Integrated use of time frequency wavelet decompositions for fault location in distribution networks: theory and experimental validation," *IEEE Transactions on Power Delivery*, vol. 25, n. 4, pp .3139-3146, Oct. 2010.

[17]   A. T. Johns, "New Ultra-high-speed Directional Comparison Technique for the Protection of E. H. V. Transmission Lines," *IEE Proceedings on Genereration, Transmition an Distribution*, vol. 127, n. 4, p.228-239, Jul. 1980.

[18]   F. V. Lopes, D. Fernandes Jr, W. L. A. Neves, "Fault Location on Transmission Lines Based on Travelling Waves," *in Proc. 2011 International Conference on Power Systems Transients,* 2011